Neuron
Article

Dynamic Ensemble Odor Coding in the Mammalian Olfactory Bulb: Sensory Information at Different Timescales

Brice Bathellier,[1,2] Derek L. Buhl,[1,4] Riccardo Accolla,[1,3] and Alan Carleton[1,*]
[1]Flavour Perception Group
[2]Laboratory of Computational Neuroscience
[3]Laboratory of Sensory Processing
Brain Mind Institute, Ecole Polytechnique Fédérale de Lausanne, Lausanne (EPFL), CH-1015, Switzerland
[4]Present address: Massachusetts Institute of Technology, Cambridge, MA 02139, USA.
*Correspondence: alan.carleton@epfl.ch
DOI 10.1016/j.neuron.2008.02.011

SUMMARY

Neural firing discharges are often temporally patterned, but it is often ambiguous as to whether the temporal features of these patterns constitute a useful code. Here we show in the mouse olfactory bulb that ensembles of projection neurons respond with complex odor- and concentration-specific dynamic activity sequences developing below and above sniffing frequency. Based on this activity, almost optimal discrimination of presented odors was possible during single sniffs, consistent with reported behavioral data. Within a sniff cycle, slower features of the dynamics alone (>100 ms resolution, including mean firing rate) were sufficient for maximal discrimination. A smaller amount of information was also observed in faster features down to 20–40 ms resolution. Therefore, mitral cell ensemble activity contains information at different timescales that could be separately or complementarily exploited by downstream brain centers to make odor discriminations. Our results also support suggestive analogies in the dynamics of odor representations between insects and mammals.

INTRODUCTION

Detection and identification of odors are performed by highly conserved anatomical structures throughout the animal kingdom. In vertebrates and invertebrates, odorant molecules are sensed by a large family of olfactory receptor proteins expressed by sensory neurons. Most neurons express only one particular receptor, and their axons converge in a receptor-specific manner onto segregated anatomical structures called glomeruli both in the vertebrate olfactory bulb (OB) and in the insect antennal lobe (AL) (Mombaerts, 2004). On the anatomical level, OB and AL are commonly considered to be homologous structures, because their principal neurons (mitral cells [MCs] in the OB and projection neurons in the AL) represent the only pathway through which olfactory information is transmitted to higher brain centers, and because of the similarities shared by their circuitry (Kay and Stopfer, 2006). On the functional level, however, different theories are currently debated about the coding principles implemented in these relay networks, and there, the homology between OB and AL is far from established.

Both in OB and AL, odor-dependent changes in firing activity of the principal neurons display strong dynamics. Neuronal responses in the insect AL and the fish OB have the form of complex, but odor-specific, activity sequences that can last for more than 1 s after stimulus offset (Brown et al., 2005; Friedrich and Laurent, 2001; Mazor and Laurent, 2005; Stopfer et al., 2003; Wilson et al., 2004). In mammals, the most visible example of temporal dynamics is the periodic modulation of MC activity by the animal's breathing (Buonviso et al., 2003; Macrides and Chorover, 1972), but slower processes were also observed in single cells (Mair, 1982; Meredith, 1986). However, in the absence of population activity analysis, it is not clear to what extent the dynamic processes observed in insects relate to those observed in mammals. In addition, two important questions remain unanswered. First, what are the features or variables in these dynamics that contain information about sensory stimuli? And which of these features may actually constitute the code used by downstream brain structures to retrieve odor information?

In OB and AL, the first question aims to resolve a debate about the timescale of features relevant for odor coding. On the one hand, many studies assume explicitly or implicitly that no information is to be found beyond a coarse description of neuronal firing rates, and discard fast timescales by using long temporal averages to represent OB activity (Davison and Katz, 2007; Lin et al., 2005; Rubin and Katz, 1999; Wang et al., 2003; Zou and Buck, 2006). On the other hand, several works suggest that the odor code could be contained at higher temporal resolutions. For example, spike timing within the breathing cycle in mammals seems informative (Macrides and Chorover, 1972; Margrie and Schaefer, 2003; Schaefer et al., 2006; Scott, 2006). These studies echo others—in particular in regards to hippocampal place cells (O'Keefe and Burgess, 2005), but also in regards to several other brain systems (Hallock and Di Lorenzo, 2006; Wiener and Richmond, 1999)—that emphasize the need of accounting for fine temporal features to retrieve a maximum of nontemporal

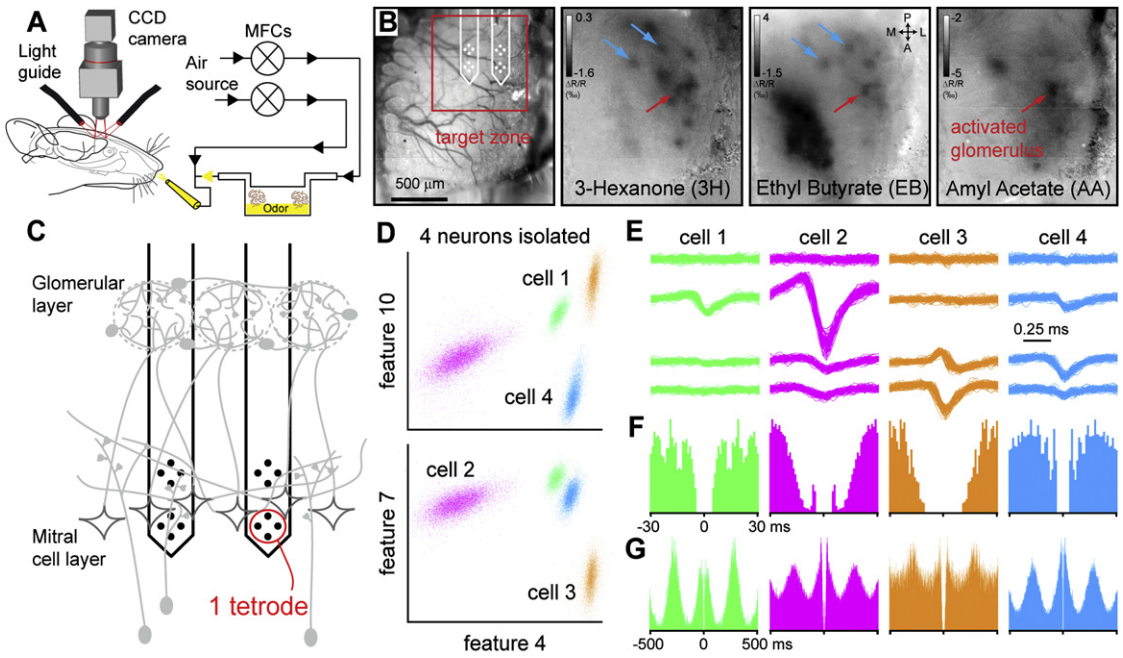

Figure 1. Targeted MC Recordings in Odor-Activated Territories

(A) Sketch of the odor delivery and intrinsic optical imaging recording setup. MFCs, mass flow controllers.

(B) Blood vessel patterns and glomerular patterns for three odors (all at 0.02) in the dorsal OB of one mouse. Red box indicates the target zone for tetrode recordings. Arrows point to a few glomeruli activated by more than one odor.

(C) Schematic positioning of the electrodes during tetrode recordings.

(D) Spike clouds of four individual neurons (different colors) isolated from the same tetrode plotted in the space of spike features. Projections on two feature planes are showed.

(E) Superposition of the first 100 spike waveforms recorded on each tetrode site for the neurons presented in (D).

(F) Autocorrelograms of the spikes trains of the four neurons for the entire recording duration, showing the refractory period of each neuron. Time bin, 1 ms.

(G) Same as (F), on a larger timescale. The oscillation period corresponds to the breathing cycle period.

information (e.g., about animal position, visual stimuli, etc) out of neural activity. Nevertheless, for the specific case of OB, no quantitative evaluation of the information contained at the different timescales of its activity has yet been conducted in live animal preparations.

In the present study we performed in vivo extracellular recordings of neural ensembles in the MC layer of the mouse OB. We show that ensemble activity has the form of complex temporal sequences developing below and above the breathing cycle timescale, which we characterize in details. Using a population activity-based odor prediction algorithm and Fourier analysis, we then evaluate the amount of information contained at different resolutions of the activity sequences. We observe that the amount of odor information is maximal in timescales close to breathing cycle period, but is also present at finer temporal resolutions.

RESULTS

MC Recordings in Odor-Activated Areas

In the OB, MC activity derives from odor-specific input maps that correspond to the activation of a subset of all glomeruli. These maps can be assessed using intrinsic imaging techniques to target MCs actually involved in the encoding of the selected test odors (Figures 1A and 1B) (Rubin and Katz, 1999). From performing imaging experiments, we could identify three odorants (3-hexanone, ethyl butyrate, amyl acetate) that consistently elicited glomeruli responses in the same zone of the dorsal OB (Figure 1B). These patterns were relatively dense and partially overlapping, corresponding to usual glomeruli maps of moderately concentrated odorants (Wachowiak and Cohen, 2001) or of the complex mixtures that constitute natural odors (Lin et al., 2006). The selection of such patterns was also intended to facilitate a direct comparison of our data with the reported high density of principal neuron activity in fish and insects (Friedrich and Laurent, 2001; Stopfer et al., 2003). Interestingly, the position of these patterns was found to be reliable across animals (Figures S1 and S2 available online). A precise zone (~900 × 900 μm, Figure 1A) could thus be defined on the basis of anatomical landmarks, in which extracellular recordings were repetitively targeted. This zone still contained roughly 150 glomeruli and therefore ~3000–5000 MCs, which were randomly sampled (see Supplemental Data). Tetrodes were lowered from the surface of the OB until the spiking activity of the MC layer was identified (Figure 1C). Single-cell activity was then separated by a standard clustering algorithm (Figures 1D–1F), and MCs were identified by usual electrophysiological criteria (see Experimental Procedures). During the experiments, animals were anaesthetized, which permitted us to obtain a regular breathing period that was comparable across trials and between animals

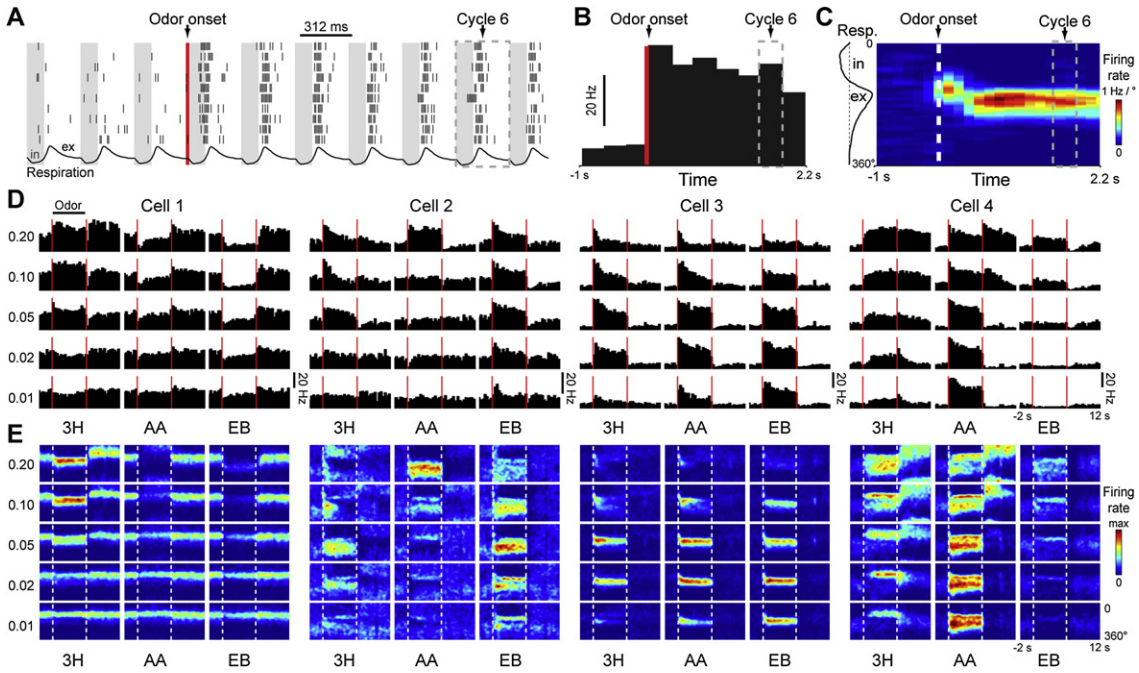

Figure 2. Odors and Concentrations Trigger Complex Firing Patterns in MCs

(A) Raster plot [Cell 3 in (D), 10 trials] of MC activity in response to amyl acetate 0.05. The duration of each breathing cycle is artificially adjusted to its average value (312 ms) to show the actual timing precision. Red bar: odor onset. in, inspiration; ex, expiration.

(B) Peristimulus time histograms (PSTH, 312 ms time bin) for the example shown in (A).

(C) Plot of the spike phase density evolution over time for the example showed in (A). For each spike, the timing from odor onset and the phase in the current breathing cycle were measured. The color code represents the number of spikes falling in square bins of 140 ms width on the time axis (x axis) and 5° width on the phase axis (y axis). To improve readability a low-pass filtering was applied with a Gaussian kernel of 2 bins.

(D) PSTH (312 ms time bin) for three odors (hexanone, 3H; ethyl butyrate, EB; amyl acetate, AA) at five concentrations (0.01 to 0.20). Four cells recorded simultaneously by the same tetrode are shown. Odor presentation (5 s) is indicated by the red bars. Time axis goes from −2 to 10 s relative to stimulus onset.

(E) Spike phase density plots for the same cells and stimuli as in (D). Color scale maxima for Cell 1 to 4: 1.0, 0.4, 1.0, and 0.5 Hz/°.

(mean 312 ms ± 32 standard deviation [SD]; n = 13 mice), allowing us to precisely follow the temporal evolution of responses.

Odor Responses Are Densely Distributed and Highly Dynamic

In a first set of experiments, we recorded a total of 101 isolated neurons in 13 freely breathing animals, during presentation of the three selected odorants at five different concentrations each (15 stimuli in total). In all cells, spiking activity was modulated by respiration (Figure 1G and Figure 2A). We plotted the activity either in histograms binned over breathing periods (Figure 2B) or in 2D plots representing the temporal evolution of the spike distribution within respiratory cycles (Figure 2C). Figures 2D and 2E show odor responses in four MCs simultaneously recorded from the same tetrode (i.e., from very spatially close locations). These examples illustrate that single-neuron firing during the 5 s stimulus application was temporally patterned, both across and within breathing cycles, with a large diversity of profiles that varied with the cell and the stimulus considered. On the slow timescale (i.e., activity averaged over breathing cycles), we could observe tonic (e.g., Figure 2D: Cell 2, AA 0.20; Cell 4, EB 0.01), phasic (Cell 1, AA 0.20; Cell 3, 3H 0.10), transient (Cell 3, AA 0.20), or delayed (Cell 4, 3H 0.02) profiles for both excitatory and inhibitory responses. On the fast timescale (i.e., dynamic activity within breathing cycles), the average and the width of spike phase distributions with respect to the breathing cycle were also diverse across cells and stimuli (Figure 2E and Figures 3A–3C) and could change over time (e.g., Figures 2C and 2E: Cell 4, AA 0.20; Cell 2, EB 0.02).

Interestingly, most neurons of the population were affected by our set of stimuli, which was probably the consequence of the spatial density of their inputs (Figure 1 and Figure S1). Comparing each breathing cycle during stimulus presentation to a baseline breathing cycle, we found that over time, each neuron responded on average to around 4 of the 15 stimuli with a significant change of either firing rate (increase or decrease) or spike phase distribution (Figure 3D). This number decreased from the beginning to the end of the stimulus presentation, indicating that at least one-fourth of the responses were transients. We considered a neuron to be responsive if it showed at least one significant rate or phase change during the entire stimulus presentation. With this criteria, 87% of the neurons responded to at least one concentration of one odor, 60% responded to two different odors, and 34% to all three odors (Figure 3E). Regarding the quality of the firing changes, it is noteworthy that in a majority of responses, only the mean firing rate was affected and pure phase changes were rare (compare green and blue curves in Figure 3D). Odors had a net excitatory effect on the MC population as about two-thirds

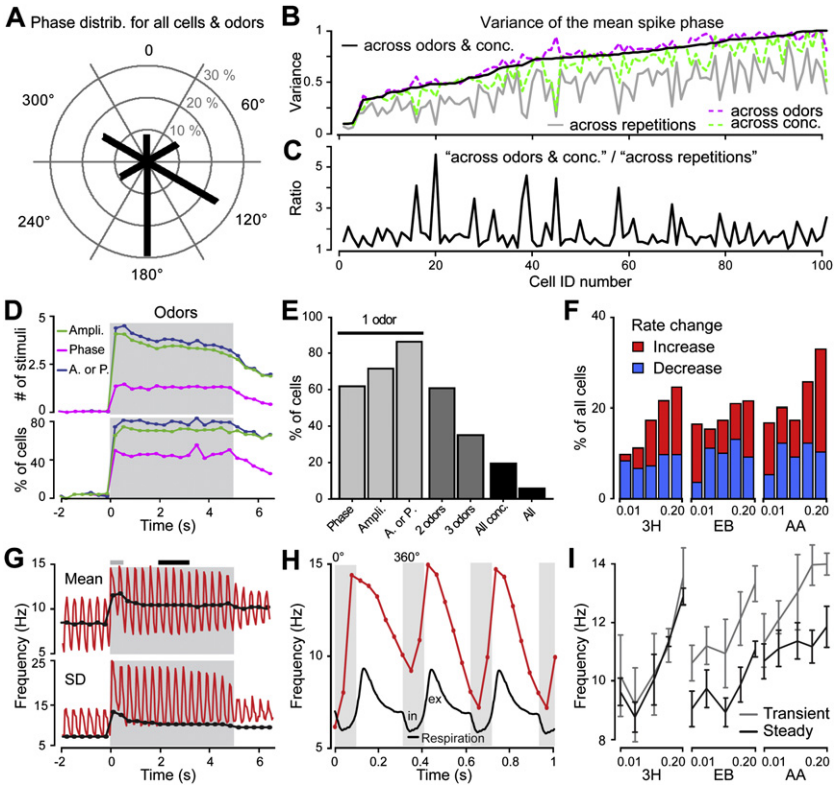

Figure 3. Population Analysis of the Responses to Odors and Concentrations

(A) Distribution of mean spike phases in the breathing cycle for all cells and stimuli.

(B and C) Variability of the spike phases for individual cells across odors and concentrations. (B) Circular variance (see Experimental Procedures) of the mean spike phases in the breathing cycle across odors (magenta), across concentrations of the same odor (green), across all odors and concentrations (black), and repetitions of the same stimulus (gray). Variance is larger across odors than across concentrations. The cells are ordered according to their "across odors and concentrations" variance. (C) Ratio of across odors and concentrations variance over across repetitions variance. The phase of individual neuron responses varies above noise when odor identity and intensity are varied.

(D) (Top) Average number of stimuli for which a statistically significant change of activity is observed in each cell and in each cycle. Cyan: phase or amplitude responses (A. or P.). Magenta and green: phase only and amplitude only. (Bottom) Fraction of the recorded cells which responded to at least 1 of the 15 stimuli.

(E) Light gray: Fraction of the cells showing at least one significant response during the entire odor presentation: phase, amplitude, or either one of them (A. or P.). Dark gray: Fraction of cells responding to at least two or to all three odors for at least one concentration. Black: fraction of cells responding to all concentrations of at least one compound (All conc.), and responding to all stimuli (All).

(F) Percentage of recorded cells responding with a significant firing rate increase (red) or decrease (blue) for each odor and concentration.

(G) (Top) Mean population firing rate averaged over the 101 recorded cells and the 15 stimuli. (Bottom) SD over the 101 cells averaged over the 15 stimuli. Black and red curves represent firing rate computed in 1 and 8 time bins per breathing cycle, respectively (~312 and 39 ms).

(H) Mean firing rate as in (G) expanded over the first three cycles after stimulus. The breathing pattern is also plotted. Gray bars indicate inspiration epochs.

(I) Mean firing rate in the first two (transient response; gray) and in the seventh to the tenth respiratory cycles (steady response; black) for each odor and concentration (represented on a logarithmic scale). Error bars represent the trial-to-trial SD.

of the rate changes corresponded to an increase (Figure 3F). Thus, the mean population firing rate increased following stimulation (Figure 3G), and this increase depended on odor concentration (Figure 3I). Interestingly, the net increase was small compared to the variability across neurons (SD in Figure 3G) or to the firing rate modulation within breathing cycles both before and during stimulation (red curves, Figures 3G and 3H). Therefore, diversity was the main characteristic of MC responses, along with broad tuning, temporal patterning, and lack of spatial homogeneity. Furthermore, no obvious single neuron coding principles emerged from the data. If some monotonic increases between firing characteristics (rate or phase) and concentration were observed, they were not the rule (Figures 2D and 2E). For example, measuring mean firing over the 5 s stimulation in the 303 odor-cell pairs, we found 85 monotonic firing increases, 42 monotonic decreases, 26 nonmonotonic evolutions, and 150 cases for which no statistically significant change of firing was observed when concentration was increased (either no response or constant response). We therefore postulated that odorant-evoked OB responses would be more efficiently described in an ensemble approach.

Characterization of Mouse OB Ensemble Dynamics

Similarly to previous studies in the insect olfactory system (Brown et al., 2005; Mazor and Laurent, 2005; Stopfer et al., 2003), we used the population vector paradigm to represent ensemble activity. We pooled all neurons recorded in different animals, assuming that they represent the same variability of neural responses as an equal number of cells recorded in a single mouse (however, results discussed below remain valid for single animals; see Figure S3). The activity of the 101 neurons was organized in 101-dimensional vectors, containing in each dimension the average firing rate of a recorded cell computed over a certain time bin (Figure 4A). The temporal evolution of population firing is thus described by vector time series for each single presentation of any odorant. Population vectors were first built using breathing cycle time bins (on average, 312 ms). One way of capturing the temporal evolution of population activity during an odor presentation is to compute the similarity between vectors of the time series (Figure 4B; similarity was measured either with the correlation coefficient [CC] or the Euclidean distance). For any stimulus, we observed three different time blocks of strongly dissimilar activity patterns (i.e., low CCs or high distances between the blocks; Figure 4B) corresponding to the resting state, the actual odor presentation, and poststimulus period. The CC values tended to be maximal (~0.8) and homogenous toward the end of the odor presentation block, suggesting a convergence to stationary states of population activity. However, the smaller CCs (~0.6) between first and

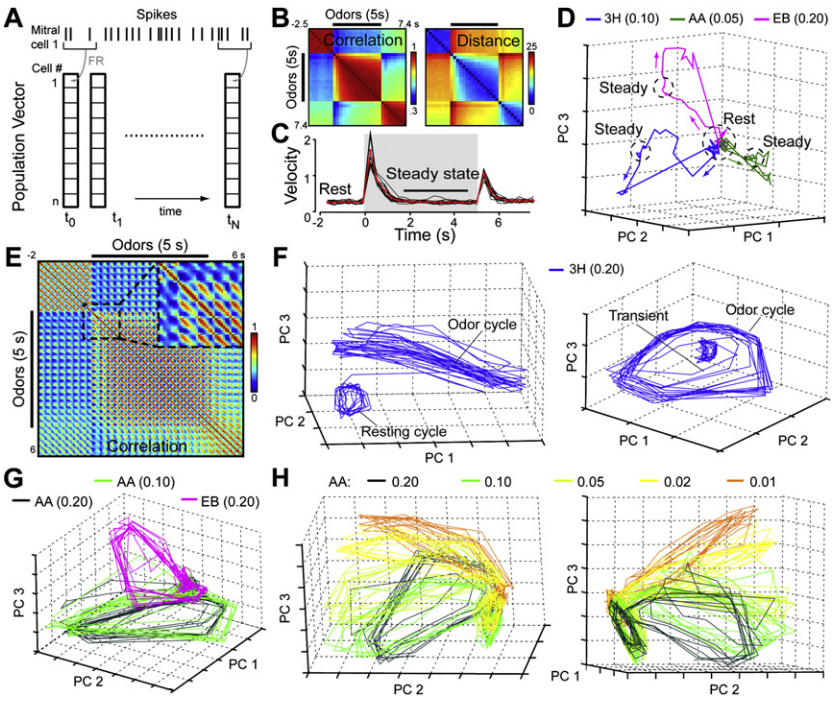

Figure 4. Population Dynamics on Slow and Fast Timescales

(A) Construction of the population vectors. For any time bin (t_0 to t_N), the n^{th} dimension of the vectors corresponded to the average firing rate (FR) of the n^{th} recorded cell.

(B) Matrices of correlation and Euclidean distance between population vectors at different time points (average over all stimuli; time bin, 312 ms).

(C) Population vector velocity (difference between consecutive 312 ms bins, in Hz per bin and per cell). Traces for all individual stimuli (black lines) and their average (red line) are shown.

(D) Average trajectories of the population vector (1 bin per cycle from −4 s to 7.4 s: trajectories are artificially closed) for three odors, visualized in the space of their first three principal components (PC). Steady states are surrounded by dashed circles.

(E) Matrix of correlation as in (B) but with 8 bins per breathing cycle. The inset shows an enlargement of a zone (1.6 s duration) around stimulus onset (dashed square).

(F) Average trajectory of the population vector (8 bins per cycle, from −2.5 to 4 s) for hexanone 0.20 and visualized in the space of its first three PCs. Two different viewing angles are shown.

(G) Trajectories as in (F) but for amyl acetate 0.10 and 0.20 and ethyl butyrate 0.20.

(H) As in (F) but for all concentrations of amyl acetate. Two different viewing angles are displayed.

last time bin of the odor presentation block (Figure 4B) also revealed a degree of activity reorganization within this epoch. These dynamic transitions could be better visualized when computing the rate at which the vectors changed over time (i.e., vector velocity, representing the distance between the population vectors of consecutive time bins; Figure 4C). After a steep change at odor onset, population activity kept evolving significantly above "noise" (i.e., baseline velocity) for ~1 s, and then reached a steady state. Another transient evolution was observed at odor offset, and then the population settled in a post-stimulus state that slowly drifted back to the resting state (within ~20 s). MC ensemble responses could also be visualized as trajectories followed by the 101-dimensional vector, in which long transients linked a resting state to some odor-specific steady states (see the low dimensional representation of average trajectories in Figure 4D).

When population vectors were constructed using shorter time bins (39 ms = 8 bins per breathing cycle), even stronger dynamics were revealed inside respiratory cycles (see the large amplitude of fine scale modulations in the matrix of CCs; Figure 4E). This fast evolution of population activity reflected the sequential activation of different neurons during each cycle (i.e., MCs firing in different phases as seen in Figure 2E and Figures 3A–3C) that followed intermittent delivery of odorant molecules during inspirations. As a consequence, the steady states observed at low temporal resolution unfolded into cyclic trajectories (i.e., resting and odor cycles; Figure 4F). These cycles were linked by pseudoperiodic transients corresponding to the evolution of neuronal activity on a timescale above breathing frequency (Figure 4F and quantification in Figure S4). Trajectories and cycles also clearly appeared to be stimulus dependant. Interestingly, they were more similar for close odor intensities than for different odor identities or more distant intensities (see Figures 4G and 4H and the quantification of intertrajectory distances in Figure S5). However, despite this continuity with respect to odor intensity, trajectories could in some cases be more different for two distant concentrations of the same odor than for two different odors (Figure S5).

Altogether, these analyses revealed that the complex activity of single neurons can be in fact interpreted on the level of neural ensemble as slowly converging, odor-dependant cyclic dynamics (the actual degree of odor specificity of trajectories is evaluated in Figure 6). Importantly, analyses of population vector similarity along time (Figures 4B and 4E) showed that these dynamics are not simply the result of global firing modulations but in fact corresponded to sequences of different population activity patterns. In theses sequences, both the subsets of excited or inhibited neurons (Figure 2 and Figures 3E and 3F) and the timing of some cells firing (Figure 3B) were stimulus specific. It was however clear that OB dynamics were entrained by the animals' respiration. Thus, they cannot be fully characterized without accounting for variations in the sniffing frequency.

Robustness of Population Dynamics with Respect to Changes in Breathing Frequency

The breathing rhythm is not a constant clock in mammals; for instance, rodents are known to sniff much faster during active odor sampling than during normal behavior (Uchida and Mainen, 2003). It is therefore crucial to understand how OB activity evolves when sniffing frequency is varied. For this reason, we performed recordings in tracheotomized mice and imposed

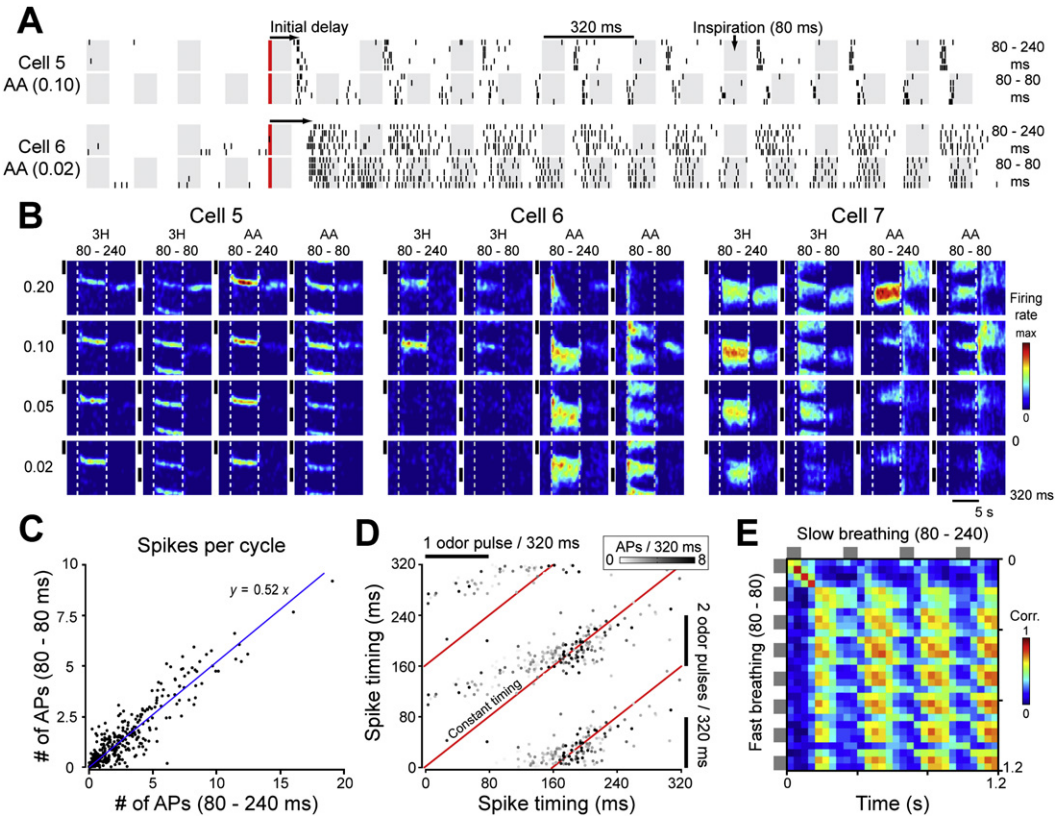

Figure 5. Effect of Breathing Frequency on OB Temporal Dynamics

(A) Raster plots of two neurons showing slow and fast breathing frequencies. The red bars and gray boxes indicate odor onset and inspirations, respectively.

(B) Spike timing density plots against time for 3-hexanone (3H) and amyl acetate (AA) at four concentrations. Timing (y axis) is computed within successive 320 ms periods that include one inspiration (starting at timing 0) for slow breathing and two inspirations (starting at timing 0 and 160 ms) for fast breathing (80 ms inspiration to 80 ms expiration). Dashed lines indicate odor onset and offset. Black lines represent inspirations. Color scale maxima for Cell 5 to Cell 7: 0.9, 0.7, and 1.0 Hz/°.

(C) Number of spikes per cycle for slow and fast breathing plotted against each other. Each point represents a measure for one recorded cell (n = 44) and one of the eight stimuli. The blue line is a linear regression of the data.

(D) Average timing of single MC spikes with respect to inspiration onset in the fast and slow cycles, plotted against each other. Each point stands for one cell and one stimulus. For clarity, two fast cycles are represented, so that spike timing can be compared over a 320 ms period. The red line represents constant timing between slow and fast cycles. The color code indicates the average number of spikes emitted for each cell-stimulus pair.

(E) Correlation matrix between population vector time series of the slow and fast breathing cycle, averaged over all stimuli.

an artificial breathing cycle. In these experiments, 44 neurons were recorded in four mice, and only two odorants (amyl acetate, 3-hexanone) were presented at four concentrations and with two different breathing cycle durations. The timing of the slower cycle (80 ms inspiration, 240 ms expiration, 3.125 Hz) was chosen to mimic the breathing of anaesthetized animals and awake animals at rest, while the faster (80 ms inspiration, 80 ms expiration, 6.25 Hz) was meant to approach the fast sniffing regime observed during active sampling (Uchida and Mainen, 2003). In between odor pulses, the artificial respiration was always set on the slow cycle mode. The switch between fast and slow breathing (when needed) was synchronized with odor onset, in such a way that the first inspiration pulse after odor onset could not be differentiated (based on the sequence of preceding pulses) between slow and fast breathing. As a consequence, for both frequencies, cells responded exactly in the same manner to this first pulse, with a robust stimulus-specific initial delay (see raster in Figure 5A). Then, spiking activity started to differ between slow and fast breathing after the onset of the second inspiration pulse (Figure 5A). These differences concerned both the number (e.g., Figure 5A, Cell 6) and the average timing (e.g., Cell 5) of spikes fired in a cycle (see also Figure 5B) and increased during the transient phase of the dynamics to finally settle after ~1 s when the dynamics across breathing cycles (i.e., slow dynamics) have converged. A full quantification of these differences for each neuron and each stimulus is showed in Figures 5C and 5D (1 to 5 s after odor onset). Figure 5C shows that on average the number of spikes per cycle was divided by two when sniffing frequency was doubled. However, a strong variability around this average indicated that this downscaling was not fully homogenous in the population of neurons. In addition, the average timing of spikes with respect to inspiration onset was not constant between fast and slow breathing, although the most evident deviations from constant timing were restricted

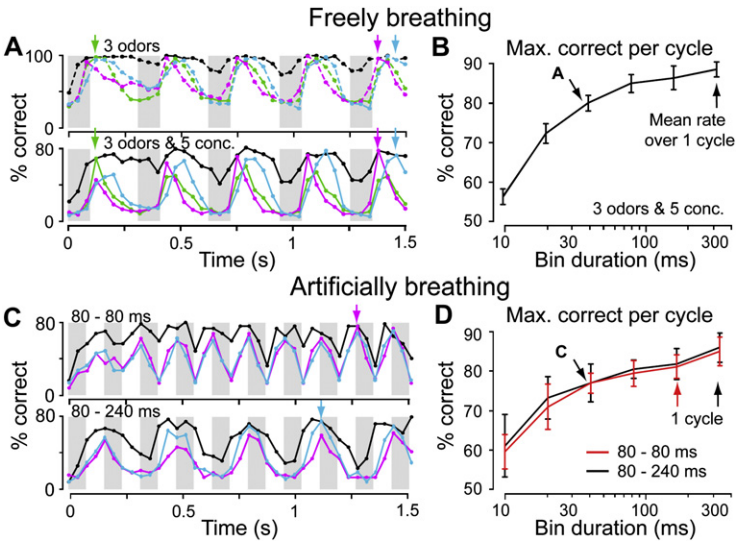

Figure 6. Information Content of Population Activity over Time

(A) Classification performance over time for odor identity only (top) or for odor identity and intensity (bottom) in freely breathing animals. Black line: the classifier is derived from the same time bin as the test trials. Colored lines: the classifier is derived from a fixed time bin indicated by the associated vertical arrow. Gray rectangles indicate inspirations.

(B) Average of the maximum classification success measured in different breathing cycles when time bin duration is varied. Error bars = SD across 15 breathing cycles after odor onset.

(C) Classification performance over time for odor identity and intensity in artificially breathing animals. Black line: the classifier is derived from the same time bin and the same breathing frequency as the test trials. Colored lines: the classifier is derived from a fixed time bin in either the fast (magenta) or the slow (blue) breathing data set as indicated by the associated vertical arrow.

(D) Same as (B) for slow (black) and fast (red) frequencies. Error bars = SD across 15 and 30 breathing cycles after odor onset, for slow and fast breathing frequencies, respectively.

to responses falling early in the slow breathing cycle (Figure 5D; Cell 5 in Figure 5A). Therefore, both the amplitude and the timing of individual cell responses were dynamically adjusted according to breathing frequency. However, when comparing population activity sequences time-by-time for slow and fast breathing, ensemble responses appeared highly correlated (CC ~0.75) in certain time windows (~between 140 ms and 240 ms after inspiration onset in the slow cycle, corresponding to the early expiration phase of the breathing cycle; see CC matrix in Figure 5E), but correlation was low at the end of expiration and the beginning of inspiration, when the population firing rate decreases substantially. The large CC can be explained by two facts. First, the time window for which CCs are high corresponds to the time window in which the timing of individual responses is least modified (Figure 5D). Second, a global downscaling of firing rates (as we approximately observed in Figure 5C) does not change the relative distribution of firing rates within the population, which is in fact what the CC measures. We could conclude that over a certain time window and despite dynamical adjustments, the distribution of activity in the population was robust to variations of the breathing frequency.

Time-Dependent Discrimination Power of Ensemble Trajectories

Beyond the description of OB ensemble dynamics, it is important to determine how much information about odorants is carried by this complex ensemble activity, and which code could be used to extract it. The information conveyed by a specific neural code represents the quality of the prediction of any specific stimulus (among all possible) given a single observation of the underlying neural activity. In the OB, since the population activity constantly evolves during the stimulus presentation, one can wonder how much information it contains at different time steps. For this evaluation, we used a classification algorithm based on population vector similarity (see Experimental Procedures), and tested data sets for which animals were freely breathing (101 cells, three odors at five concentrations) and for which they were tracheotomized (44 cells, two odors at four concentrations). Considering the population of 101 neurons recorded in freely breathing animals, the algorithm run in each 39 ms time bins independently classified odor identity only and identity plus intensity with up to 100% and 83% success, respectively (Figure 6A, black lines). The maximum classification success for odor identity and intensity obtained in a cycle increased with bin duration to reach approximately 90% for the entire cycle duration (87% ± 3%, Figure 6B). A similar level of maximal performance was obtained in all breathing cycles, but only in a specific time window roughly corresponding to the expiration phase of the breathing cycle (see plateau of high classification success, Figure 6A). Therefore, fast, but not slow (i.e., within, but not across, breathing cycles), dynamics modulated the amount of information that we could retrieve from population activity. Because the classification success (or information) was similar in different periods, one might think that the underlying cell assemblies necessary for coding are similar. This was not the case. If we applied the classification algorithm using fixed reference templates (called classifiers) of population activity taken in a particular time bin in a breathing cycle (i.e., corresponding to a particular cycle phase; colored arrows in Figure 6A), we found that the classification success in other time bins was strongly fluctuating within and across breathing cycles. Classification appeared to be maximal only for time bins corresponding to the same cycle phase of the classifier. In addition, classifiers selected in the transient regime (approximately the first two respiratory cycles) could not efficiently decode activity in the steady odor cycle regime and vice versa (colored lines, Figure 6A). Thus, within and across breathing cycles dynamics distributed odor information in different ensemble activity configurations over time. In the case of artificially breathing animals, similar results were observed (Figures 6C and 6D). In addition, we observed that ensemble activity during fast breathing could efficiently classify activity during slow breathing, and vice versa (see colored lines and arrows in Figure 6C). However, consistent with the analysis illustrated in Figure 5E, the best cross-classification efficiency was only observed if classifiers were chosen in the 140–240 ms time window in which correlation of

population activity between slow and fast breathing was high. This demonstrated that a code based on population activity in ~40 ms time bins would be robust to changes in the breathing frequency. But note that this is also true for larger time bins (e.g., 160 ms bins; Figure S6).

Altogether these analyses showed that averaged firing activity in single epochs of the population trajectories could robustly and efficiently code for odors and concentration. However, because different epochs represented dissimilar states of population activity, the time course of activity (i.e., the combination of different epochs) could also be part of the odor code. To precisely address this possibility, it is necessary to evaluate on which timescales temporal features of the response actually contain some information about the stimulus.

Evaluation of Information at Different Timescales

The information contained at different timescales in a neural activity sequence can be captured by Fourier analysis, which decomposes the signal into its variations at different frequencies. For a sequence of activity spanning a breathing cycle, we can extract for each cell a series of Fourier coefficients representing increasingly fast fluctuations of the signal that are robustly locked to the cycle in different trials (this excludes temporal coincidences between neurons that occur with some jitter with respect to breathing). The first coefficient (frequency 0) gives the mean firing rate during the respiratory cycle. The second coefficient (breathing frequency) contains the mean phase and roughly the amplitude of activity modulation during breathing. Subsequent coefficients contain the so-called higher harmonics that correspond to the precise shape of the firing burst in the cycle (e.g., width and multiple firing peaks, if any). We could specifically evaluate the information present in the neural population at a particular timescale or frequency by constructing the population vectors with the Fourier coefficients for that frequency measured in each cell (Figures 7A and 7B). The two first Fourier coefficients yielded the highest classification performance, which then progressively decreased when smaller timesscales were considered. However, some information about the stimulus was still available up to 20–40 Hz resolution (i.e., 50 to 25 ms timescale, Figures 7A and 7B). It is noteworthy that higher resolutions were more informative in the artificially breathing (Figure 7A) than freely breathing experiments (Figure 7B). This might be the consequence of breathing frequency fluctuations that introduce additional variability in faster scales. Interestingly, the classification performance obtained with the lower resolutions (first and second Fourier coefficient) was very high (87% and 91% for freely breathing animals, and approximately 80% for artificially breathing animals). Adding higher-resolution features (discrimination based on all Fourier coefficients; Figure 7A and 7B, "All" on x axis) little improved these performances. Therefore, information contained in fast firing fluctuations locked to breathing was not crucial for classification of the proposed odor set with our readout method, which nevertheless would not preclude them to be useful for a more difficult discrimination task or to be used by downstream brain centers.

We complemented this general analysis with evaluations of information in some specific temporal features that have been proposed to be involved in coding, but are not specifically isolated by Fourier coefficients. For instance, latency of the first spike in the breathing cycle (Figure 7C) was suggested to be a potential odor code (Margrie and Schaefer, 2003). We observed that this feature indeed contained odor information (on average, 46% classification success as compared with a 6.7% chance level in freely breathing animals, Figure 7D; note that stimulus-dependant properties of the latency were similar to those observed in the latter study; Figure S7), but less information than other features such as mean firing rate. A similar observation was made for the mean spike phase in the breathing cycle, a part of the second Fourier coefficient (70% classification success on average; Figure 7D). Altogether these analyses showed that averaged activity in single epochs of the population trajectories could robustly and efficiently code for odors and concentration for at least the moderately difficult discrimination tasks proposed in our experiments.

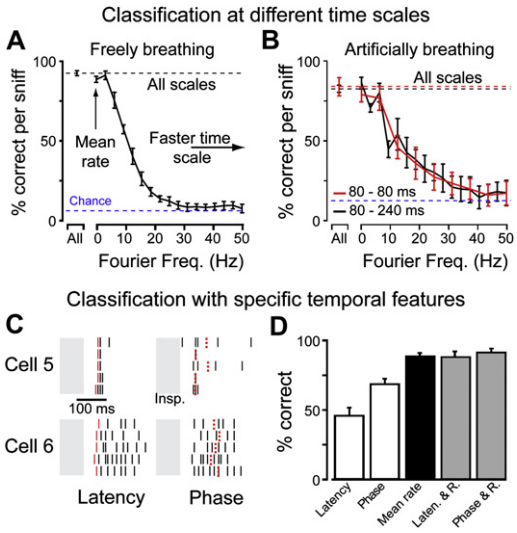

Figure 7. Information Contained at Different Timescales

(A) (Top) Percentage of success for classifications based on temporal details at different timescales below respiration frequency. The sequence of population activity in a breathing cycle is decomposed in Fourier coefficients for the 16 first integer multiples of the breathing frequency ($f_n = k.f_{breathing}$). Each coefficient selectively captures the temporal details that have a typical duration corresponding to the inverse of the Fourier frequency. We plotted the classification success for different coefficients. The mean firing rate in the cycle corresponds to $k = 0$. Classification success when all timescales (i.e., Fourier coefficients) are used corresponds to "All". Error bars = SD across 15 breathing cycles after odor onset.

(B) Same as (A) for both fast (red line) and slow (black line) breathing in artificially breathing animals. Error bars = SD across 15 and 30 breathing cycles after odor onset, for slow and fast breathing frequencies, respectively.

(C) Examples of firing latencies (red lines) and mean firing phase (red dotted lines) for two neurons induced by an odor in different trials and shown in two consecutive respiratory cycles.

(D) Classification performance for five different coding schemes over each breathing cycle. White: discrimination based only on firing latency or mean spike phase measured in all cells in each breathing cycle. Black: mean firing rate over a breathing cycle. Gray: mixed schemes; mean firing rate combined to firing latency or to mean phase. Error bars = SD over the 15 cycles of the stimulus presentation.

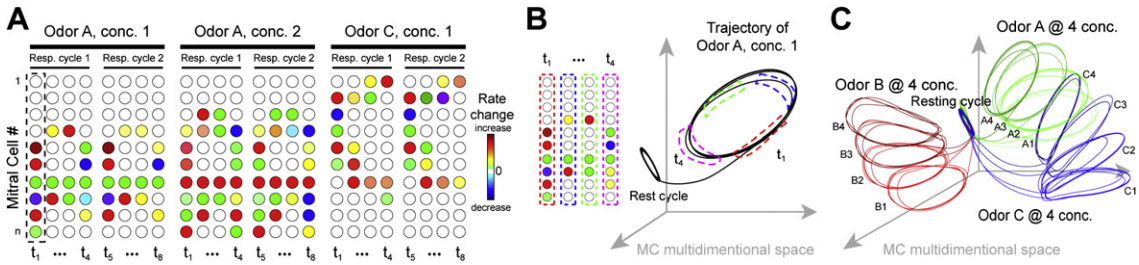

Figure 8. Schematic Representation of OB Population Dynamics

(A) MC populations respond to odors with specific activity sequences. Distribution of firing rates changes strongly over time within breathing cycles, while few relative changes are observed across cycles.

(B) The population activity can be visualized by trajectories in the MC multidimensional space. After odor onset, the population activity leaves its resting cycle state to reach an odor-specific cyclic trajectory via an ~1 s pseudoperiodic transient.

(C) If there is continuity between the cyclic trajectories observed for two close concentrations of the same odorant, odor cycles could in some cases be more different for two distant concentrations of the same odor than for different odors.

DISCUSSION

In this study, we recorded and analyzed MC activity in response to different odors and concentrations. This activity was dynamic, both at timescales below and above breathing cycle (Figure 2 and Figure 8A). Single-cell firing activity was variable across odors and concentrations (Figure 3) and was modified by the frequency of breathing (Figure 5). We observed in many cells clear phase changes across odors and concentrations (Figure 3). Odorant stimuli evoked odor-specific sequences of activated cells and therefore appeared to be well characterized by a neuronal ensemble description. We also showed that ensemble activity changed in intensity over time. The average population firing rate was modulated during each breathing cycle, but also slowly decreased from one cycle to another before settling in a steady state (Figures 3E and 3F). These global variations were not homogenously spread over the population but happened in parallel to a strong reshaping of population activity patterns on timescales below and above breathing frequency (Figure 4 and Figure 8B). Finally, we found that ensemble activity contained sensory stimuli information at different timescales that could be used for efficient coding.

Ensemble Dynamics in the Mouse OB: Comparison with Insects

Interestingly, complex temporal dynamics have also been observed in the AL of several insects (Lei et al., 2004; Stopfer et al., 2003; Wilson et al., 2004; Mazor and Laurent, 2005), and have been best characterized in the locust AL. The cyclic dynamics observed in mice are due to breathing, which imposes a periodic excitation to the olfactory epithelium and thereby to the OB. When a periodic input is given to a locust, such as rapid sequences of odor pulses, then cyclic dynamics are also observed (Brown et al., 2005), and they consist of stimulus-specific sequences of brief neuronal firing locked to odor pulses that resemble OB activity within breathing cycles. This cyclic activity also exhibits a slow transient, because population activity after the first odor pulse significantly differs from activity after subsequent pulses (Brown et al., 2005). Two other analogies between the ensemble representations of odors in the locust AL and the mouse OB are the invariance with respect to variations of pulse frequency (Brown et al., 2005; Figure 5) and the continuity between representations of close odor concentration (Stopfer et al., 2003; Figure 4H and Figure 8C). All these analogies suggest that odor coding in these two homologous but evolutionary distant structures may be similar in some respects. They also suggest that the underlying mechanisms of ensemble activity dynamics may be comparable. Several potentially important processes have already been identified in both insects and mammals. First, the heterogeneity of OB input latencies across glomeruli (Scott, 2006; Spors et al., 2006) and their intrinsic filtering properties (Verhagen et al., 2007) could in part explain the sequential activation of different MCs and the overall decrease of activity over time. Interestingly, these features seem also to be present in the input to insect AL (Brown et al., 2005; Hallem and Carlson, 2006). However, they are unlikely to explain alone all observed phenomena, like the slow increase in firing rate over time observed in some cells (e.g., Figure 2D; Cell 3, 3-hexanone), or in some cases, the increase of firing delays in each breathing cycle when concentration is increased (e.g., Figure 2E; Cell 1, 3-hexanone; olfactory receptor latencies are expected to decrease with odor intensity). In insects, temporal patterning in the AL occurs in the absence of input dynamics (Wehr and Laurent, 1999). Other potentially involved mechanisms are the lateral connections between principal cells, both inhibitory (Isaacson and Strowbridge, 1998) and excitatory (Didier et al., 2001; Isaacson, 1999; Shang et al., 2007), and plasticity mechanisms (Stopfer and Laurent, 1999). Lateral inhibition has been long proposed to shape OB outputs across glomeruli (Mori and Shepherd, 1994; Yokoi et al., 1995), and several studies have shown that the slow dynamics of AL activity was dependent on a slow lateral inhibitory process (Bazhenov et al., 2001; Wilson and Laurent, 2005) that is also present in the OB (Isaacson and Strowbridge, 1998). Short-term memory in olfactory networks, which in the locust occurs during presentation of repetitive or prolonged odor pulses (Stopfer and Laurent, 1999), could also explain the slow transient and convergence of the population response toward a steady state that we observed across breathing cycles in mice. Interestingly, a model of AL suggests that plasticity of both excitatory and inhibitory synapses is necessary to best explain short-term memory in the AL (Bazhenov et al., 2005).

Odor Information Is Present at Different Timescales of the Dynamics

The existence of complex dynamics in the OB raises the question of which features of this activity actually contain odorant information. We first observed that at any instant of each breathing cycle (during odor presentation), some information can be extracted by using a measure of firing rate in a time bin. The quantity of information we could retrieve (i.e., the quality of the discrimination that our algorithm could perform) depended on time and was optimal during the expiration phase (roughly 140 to 240 ms after inspiration onset; Figure 6). When the width of the time bin was increased, discrimination was improved. However, this readout method intrinsically discarded temporal features of the dynamics. Using a different approach based on Fourier analysis, we could evaluate that these temporal details actually contain information down to a timescale of 20–40 ms. The largest amount of information was found in lower-resolution details (i.e., first Fourier coefficients) that correspond to the mean firing rate in the cycle and to the amplitude and mean phase of activity modulation at breathing frequency (but note that the phase in itself was less informative that the mean firing rate; Figure 7D). Information extracted from the higher harmonics, representing the precise shape of the activity modulation, was lower but nonnegligible (Figure 7). Because all these temporal features are below the sniffing frequency, that is, below odor sampling rate, they could be part of a code, which despite its temporal nature would be fast enough to track all fluctuations of the stimulus that the animal can actually access. Importantly, because we used the breathing cycle as a time clock to resynchronize activity recorded in different animals, our approach could not capture temporal coincidences between the activities of neurons that were not synchronized to breathing. Therefore, part of the temporal information was still discarded, a deficit that should be considered in further studies. With this limitation, the largest amount of information was found in lower-resolution details.

The sniffing frequency is not fixed in mammals. For instance, awake rodents actively control odor sampling and often increase sniffing frequency during olfactory perception (Uchida and Mainen, 2003). On the one hand, the advantage of breathing more rapidly could lay in maintaining the response for a longer time in its most informative state (Figure 6). On the other hand, we showed that breathing variations modify to some extent the time course of responses (e.g., spike timing in the breathing cycle; Figure 5A). Odor classification based on full description of activity sequences (i.e., including temporal features) appeared in our data set to be less robust to changes in sniffing speed than when based on mean firing rate (see Figure S6). This might represent a practical difficulty for implementing a temporal code in all behavioral situations. In addition, recent observations comparing OB activity between awake and anaesthetized conditions show that in the awake state, fast temporal patterns (i.e., locking to sniffing) are less prominent (Rinberg et al., 2006a). One could speculate that this can reduce the potential contribution of fast temporal features in the actual odor code. Based on our results, the actual impact of fast features on discrimination efficiency is low. We observe that fast features improve little over the information measured in slow features. However, this could be due both to the choice of the stimulus set, which could represent a discrimination task too simple for fast features to be of any use, and to the limitations of our algorithm, which, like any readout algorithm, provides only a lower bound estimation on the actual information present in the data. In conclusion, while our results indicate that different timescales of the response can be used for odor discrimination, further study is required to determine if slow and fast features give complementary or overlapping information.

Decoding of OB Activity in the Brain

Ultimately, what should be termed "odor code" in the OB is simply whichever aspects of activity are used by downstream brain structures to link sensory information to an adequate behavior of the animal. Unfortunately, little is known about the processes occurring in areas downstream of the OB during olfactory perception. A crucial question is whether processing mechanisms in the target areas work with a resolution sufficient to preserve temporal details. Recordings in the piriform cortex recently showed temporally patterned response both on the breathing cycle timescale and above (Rennaker et al., 2007), suggesting temporal features present in the bulb could be preserved at the cortical level. This seems to be clearly the case in the insect analog of piriform cortex (the mushroom body), where integration of downstream activity clearly occurs on a short timescale (~50 ms) (Perez-Orive et al., 2002). However, neuronal integration mechanisms in the mushroom body only take into account downstream activity in single ~50 ms epochs and not activity from the combination of several epochs (Perez-Orive et al., 2002), suggesting that the mushroom body propagates, but may not readily interpret, information from temporal features. It is therefore still an open question in insects and mammals whether fast temporal features are part of the code read at higher brain levels. It is also important to note here that some temporal features were not considered in the study. In particular, it has also been shown that synchrony with gamma-band oscillations can also play an important role in the reading out of AL and OB activity (Mazor and Laurent, 2005; Friedrich et al., 2004; Perez-Orive et al., 2002). If our analyses took into account any synchronization with respect to the breathing cycle, they did not include gamma synchrony, essentially because gamma oscillations do not constitute a robust clock that one can resynchronize among different animals. However, since prominent gamma activity is regularly observed in the mammalian OB (Lagier et al., 2004) and in correlation with odor perception (Beshel et al., 2007), the question of its role in olfactory coding also needs to be fully addressed in the future.

Not only the temporal aspects but also spatial distribution of OB responses is a crucial issue in odor coding theories. In this respect, our recordings targeted densely activated, but not necessarily the most specific, regions of the OB, which may contrast with the sparse activity reported previously using low odor concentration or in awake animals (Davison and Katz, 2007; Rinberg et al., 2006a). Particularly puzzling is the issue of the state dependence of response density (Rinberg et al., 2006a). It seems that awake activity is characterized by a higher activity level and an increased noise that can also be due, to some extent, to nonassessed contextual modulations (Kay and Laurent, 1999). Despite

these global changes, which can explain the reduced response density, the overall dynamic properties may still be preserved. Unfortunately, the level of details in the description of state dependence does not allow us to infer how exactly population dynamics are affected. Though our data were obtained in anaesthetized preparations, they agree fairly well with several behavioral observations. We show that accurate odor and concentration discrimination could be achieved on a single trial basis within a few hundredths of a millisecond (depending on the difficulty of the task, i.e., identity only versus identity and concentration; Figure 6A), which agrees with the rapidity of rodent odor discrimination (Abraham et al., 2004; Rinberg et al., 2006b; Uchida and Mainen, 2003). Second, discrimination using our population-based approach was only relying on a small part of the bulb, consistent with the robustness of olfactory discrimination to the removal of most glomeruli, and suggesting the existence of largely distributed information in the OB (McBride and Slotnick, 2006). Here we show that this distributed information can be retrieved by combining the activity of randomly pooled ensembles of MCs. Although this idea was applied here in a somewhat artificial fashion, it is in fact well in agreement with the anatomical organization of feedforward projections from the OB (or AL) to the piriform cortex (or the mushroom body) that are built so that information from different glomerular inputs can be heavily combined in cortical neurons (Jortner et al., 2007; Zou and Buck, 2006).

EXPERIMENTAL PROCEDURES

Animal Preparation

All experiments were performed on C57BL/6J mice (6 to 13 weeks of age), and were in accordance with the Swiss Federal Laws. Mice were urethane anesthetized (1.5 g/kg i.p.) and body temperature was kept to ~37°C using a heating pad (FHC, Bowdoinham, ME).

In one set of experiments, animals were freely breathing. Respiration was monitored using a magnet attached to the animal's thorax and a Hall-effect probe (SS94A1, Honeywell, MN). Calibration experiments using a directional air flow sensor (AWM2100V, Honeywell, MN) placed in front of the nose showed that the position of inspiration and expiration could precisely be deduced from the magnetic signal, which followed thorax displacements. Delay between air flow and magnetic signals was below 10 ms. Over the 13 mice used for electrophysiology, we observed an average breathing cycle period of 312 ms with an interanimal SD of 32 ms and an average SD of 20 ms within animals.

In another set of experiments, animals were tracheotomized and an artificial respiration was connected to the upper part of the trachea to control air flow in the nose. Inspirations and expirations were emulated by pulses of negative and positive pressure. Air flow was adjusted to match a value of 150 ml/min in both directions.

Odor Delivery and Experimental Protocol

All odors (amyl acetate, ethyl butyrate, 3-hexanone, and methyl benzoate) were from Sigma-Aldrich. Each stimulus was repeated between 10 and 15 times in freely breathing animals and 5 times in tracheotomized animals. Odors were delivered through a custom-made olfactometer during animal's expiration (odor onset was the onset of the first inspiration after delivery). A carrier flow passed through small bottles containing 5 ml pure odorant (saturated vapor) and was diluted with cleaned dry air before being sent to the nose. The total flow was constant (0.4 l/min). Computer-controlled flow controllers and electromagnetic valves allowed precise adjustment of dilution, proportion of odorants, and timing. To obtain a stable odor concentration during the entire stimulus application, we ensured that flows were stationary with a 5 s preloading of the delivery system (this duration was assessed by offline flow measurements). All concentrations are expressed as the fraction of the pure odor flow (for example, a concentration of 0.1 means that the odor flow was diluted ten times in the carrier flow). Because odors were delivered ~1 cm away from the animal's nose, these values overestimate concentrations actually reaching the nasal cavity.

In Vivo Imaging

Intrinsic signal imaging was conducted as described elsewhere (Bathellier et al., 2007) and is presented in Supplementary Materials.

In Vivo Electrophysiological Recordings and Spike Sorting

A 2 mm window was drilled above the OB and dura mater was opened (the cisterna magna was then punctured and drained to decrease brain pulsation). One or two silicon-based recording electrodes (# a2x2-tet, NeuroNexus Technologies, Ann Arbor, MI) were inserted. The skull cavity was filled with a mixture of wax and paraffin to protect the brain from drying. Electrodes were lowered vertically in the target zone identified by imaging (Figure 1B) until the dorsal MC layer (MCL) was reached. The MCL was clearly identifiable by its strong extracellular spiking activity restricted to a 100–150 μm narrow band, which contrasted with the much less prominent spiking activity in the external plexiform and the granule cell layer (Buonviso et al., 2003; Kay and Laurent, 1999; Rinberg et al., 2006a). In this respect, it must be noted that our recording electrodes had low impedances (1 to 4 MΩ at 1 kHz). Stability and reasonable size of the extracellular spike with respect to background noise are two necessary conditions for single-cell identification (clustering, see below), which in the case of low impedance electrodes could only be fulfilled by MCs and tufted cells (the larger cells in the OB), as observed by others in mice (Rinberg et al., 2006a) and in rat (Buonviso et al., 2003; Kay and Laurent, 1999). As a confirmation, we detected almost no activity in the granule cell layer, which contains a large density of small neurons.

Wide-band field potentials were amplified (100×) and band-pass filtered (0.1 Hz to 9 kHz). All data was digitized at 32556 Hz with the Cheetah Digital Lynx system (Neuralynx, Tucson, AZ). During a recording session, odors were presented in a pseudorandom order with 30 s interstimuli intervals.

Spike detection and identification of individual neurons was performed according to a standard procedure extensively described elsewhere (Csicsvari et al., 1998; Harris et al., 2000). Spikes were detected by a threshold on the high-pass filtered signal, decomposed in 16 features, and automatically clustered by the KlustaKwick software (Harris et al., 2000). Obtained clusters were manually merged in Klusters software (Hazan et al., 2006) when they showed a clear refractory period in the cross-correlation of their spike trains. Individual neurons were finally identified as the clusters showing a clean refractory period in their autocorrelation (Figure 1F). All subsequent analyses and statistics were calculated using custom scripts written for Matlab (MathWorks, Inc., Natick, MA) or C.

Statistical Analysis of Single-Cell Responses and Timing Measure

Variability of the spike phases for individual cells was assessed using circular variance (Figures 3B and 3C) that is equal to 1 – R, where R is the resultant length of the phase difference vectors (Batschelet, 1981). The difference vector contains all pairwise differences between individual repetitions of each distinct group (i.e., each of the 3 odors irrespective to concentrations, each of the five concentrations of the same odor, or each of the 15 odors and concentrations). For each cell, only stimuli for which the spike distribution in the breathing cycle was nonuniform (Rayleigh test, $p < 0.05$) were put in the analysis.

Changes of firing properties relative to baseline (Figure 3) were assessed by two nonparametric tests repeated in the 15 respiratory cycles spanning stimulus presentation and for all 15 stimuli. We used the Wilcoxon rank sum test for spike count distributions and the circular statistics Mardia-Watson-Wheeler test (Batschelet, 1981) for phase distributions. The α value was set to 0.01, but we applied a Bonferroni correction for multiple testing (division by the number of tests performed for each cell, i.e., 15 for cycle by cycle analysis and 225 for entire stimulus duration) so that all resulting percentages could not be overestimated by more than 1% (i.e., the percentage of false positives). The evaluation of the monotony of responses with respect to concentration increases was done by measuring the differences between mean firings (over 5 s) for

successive concentrations. If all statistically significant differences (Wilcoxon rank sum test, $p < 0.01$, with correction for multiple testing) had the same sign, response evolution was classified as monotonic. In Figure 5D, average timing was defined as $T \tan^{-1}(\phi_m) / (2\pi)$, where ϕ_m stands for the mean phase of spikes in the breathing cycle (phase 0 was inspiration onset) and T is cycle duration.

Population Vector Construction and Analysis

We represented the population activity as a multidimensional vector in which each line contained the firing rate of a given neuron. Firing rate was computed over fixed time bins (312 ms duration, not aligned to breathing cycles), "cycle bins" (1 bin per breathing cycle; variable duration but 312 ms on average), or "phase bins" (8 bins per cycle; 39 ms in average). Because of the regularity of the breathing, fixed 312 ms bins and cycle bins gave very similar results in terms of population dynamics, the only visible difference being that dynamical responses to odor offset were sharper with fixed bins (because it avoided small temporal drifts). For the artificially breathing data set, we used fixed 40 ms time bins.

The vector velocity was defined as the distance between temporally successive vectors. Low dimensional representations of vector trajectories were done in the following way. For a given set of stimuli, the associated temporal sequences of vectors were pooled and decomposed into principal components (PCs). Plots of the trajectories (averaged over all trials of a stimulus) were then drawn in the space of the first three PCs. For Figure 4D, the first one, three, and eight PCs contained 13%, 33%, and 54% of the total variance, respectively. For Figures 4F–4H, they contained on average 14%, 28%, and 44% of the total variance.

Classification Algorithm

To compute classification performance, one trial per stimulus was chosen to be a test set, and the remaining trials were averaged to be template responses. The Euclidean distances between test trials and all stimuli templates were computed, and trials were assigned to the closest template (i.e., to a stimulus prediction). The CC could also be used as a distance measure, yielding very similar results. The percentage of success for odor identity and intensity was the fraction of correct assignments over the total number of assignments. For odor identity only, correct assignment corresponded to the correct odor regardless of concentration.

Templates could be drawn from the same time bin as test trials (e.g., Figure 6A, black lines), or from a fixed time bin (fixed code, e.g., Figure 6A, colored lines). For the experiment with artificial breathing, templates could also be derived from fixed time bins in the data set of one breathing frequency to classify responses obtained with the other frequency (Figure 6C).

To specifically extract the temporal features at different resolutions (Figures 7A and 7B), we built population vectors based on the Fourier coefficients of single-cell activity. Taking $A_j(t)$ to be the activity of a cell j over a breathing cycle between times 0 and T, the Fourier coefficients are:

$$C_{j,n} = \frac{1}{T}\int_0^T A_j(x)\exp(-i2\pi nx/T)dx$$

where $i = \sqrt{(-1)}$ and n is the order of the coefficient (which corresponds to frequency $f_n = n/T$). The classification algorithm uses the 101-dimensional complex vector $C_n = (C_{1,n}, C_{2,n}, \ldots, C_{101,n})$. For classification based on all timescales, the first 16 C_n values are concatenated in a 1616 dimensions vector.

To account for the phase ϕ or the latency t_f of the first spike in a cycle (Figures 7D), the mean firing rate of each cell in each cycle was multiplied by $\exp(i\phi)$ or $\exp(it_f / \pi)$. For classification with phase or latency alone, all firing rates were set to 1 in the vector.

SUPPLEMENTAL DATA

The Supplemental Data for this article can be found online at http://www.neuron.org/cgi/content/full/57/4/586/DC1/.

ACKNOWLEDGMENTS

We thank W. Gerstner, M. Giugliano, C. Petersen, and J. Poulet for helpful discussion and comments on the manuscript. This work was supported by the Brain Mind Institute of Ecole Polytechnique Fédérale de Lausanne, the Leenaards Foundation, and the network of European Neuroscience Institutes from the European Union (ENI-net).

A.C. and B.B. carried out the study conceptualization and experimental design. D.L.B. contributed to settling in vivo tetrode recordings in the laboratory. B.B. and D.L.B initiated the experimental program. B.B. performed most experiments and analysis. R.A. and A.C. contributed to the analysis. B.B. and A.C. wrote and edited the manuscript.

Received: July 13, 2007
Revised: October 5, 2007
Accepted: February 6, 2008
Published: February 27, 2008

REFERENCES

Abraham, N.M., Spors, H., Carleton, A., Margrie, T.W., Kuner, T., and Schaefer, A.T. (2004). Maintaining accuracy at the expense of speed; stimulus similarity defines odor discrimination time in mice. Neuron *44*, 865–876.

Bathellier, B., Van De Ville, D., Blu, T., Unser, M., and Carleton, A. (2007). Wavelet-based multi-resolution statistics for optical imaging signals: Application to automated detection of odour activated glomeruli in the mouse olfactory bulb. Neuroimage *34*, 1020–1035.

Batschelet, E. (1981). Circular Statistics in Biology (London: Academic Press).

Bazhenov, M., Stopfer, M., Rabinovich, M., Abarbanel, H.D., Sejnowski, T.J., and Laurent, G. (2001). Model of cellular and network mechanisms for odor-evoked temporal patterning in the locust antennal lobe. Neuron *30*, 569–581.

Bazhenov, M., Stopfer, M., Sejnowski, T.J., and Laurent, G. (2005). Fast odor learning improves reliability of odor responses in the locust antennal lobe. Neuron *46*, 483–492.

Beshel, J., Kopell, N., and Kay, L.M. (2007). Olfactory bulb gamma oscillations are enhanced with task demands. J. Neurosci. *27*, 8358–8365.

Brown, S.L., Joseph, J., and Stopfer, M. (2005). Encoding a temporally structured stimulus with a temporally structured neural representation. Nat. Neurosci. *8*, 1568–1576.

Buonviso, N., Amat, C., Litaudon, P., Roux, S., Royet, J.P., Farget, V., and Sicard, G. (2003). Rhythm sequence through the olfactory bulb layers during the time window of a respiratory cycle. Eur. J. Neurosci. *17*, 1811–1819.

Csicsvari, J., Hirase, H., Czurko, A., and Buzsaki, G. (1998). Reliability and state dependence of pyramidal cell-interneuron synapses in the hippocampus: an ensemble approach in the behaving rat. Neuron *21*, 179–189.

Davison, I.G., and Katz, L.C. (2007). Sparse and selective odor coding by mitral/tufted neurons in the main olfactory bulb. J. Neurosci. *27*, 2091–2101.

Didier, A., Carleton, A., Bjaalie, J.G., Vincent, J.D., Ottersen, O.P., Storm-Mathisen, J., and Lledo, P.M. (2001). A dendrodendritic reciprocal synapse provides a recurrent excitatory connection in the olfactory bulb. Proc. Natl. Acad. Sci. USA *98*, 6441–6446.

Friedrich, R.W., and Laurent, G. (2001). Dynamic optimization of odor representations by slow temporal patterning of mitral cell activity. Science *291*, 889–894.

Friedrich, R.W., Habermann, C.J., and Laurent, G. (2004). Multiplexing using synchrony in the zebrafish olfactory bulb. Nat. Neurosci. *7*, 862–871.

Hallem, E.A., and Carlson, J.R. (2006). Coding of odors by a receptor repertoire. Cell *125*, 143–160.

Hallock, R.M., and Di Lorenzo, P.M. (2006). Temporal coding in the gustatory system. Neurosci. Biobehav. Rev. *30*, 1145–1160.

Harris, K.D., Henze, D.A., Csicsvari, J., Hirase, H., and Buzsaki, G. (2000). Accuracy of tetrode spike separation as determined by simultaneous intracellular and extracellular measurements. J. Neurophysiol. *84*, 401–414.

Hazan, L., Zugaro, M., and Buzsaki, G. (2006). Klusters, NeuroScope, NDManager: a free software suite for neurophysiological data processing and visualization. J. Neurosci. Methods *155*, 207–216.

Isaacson, J.S. (1999). Glutamate spillover mediates excitatory transmission in the rat olfactory bulb. Neuron *23*, 377–384.

Isaacson, J.S., and Strowbridge, B.W. (1998). Olfactory reciprocal synapses: dendritic signaling in the CNS. Neuron *20*, 749–761.

Jortner, R.A., Farivar, S.S., and Laurent, G. (2007). A simple connectivity scheme for sparse coding in an olfactory system. J. Neurosci. *27*, 1659–1669.

Kay, L.M., and Laurent, G. (1999). Odor- and context-dependent modulation of mitral cell activity in behaving rats. Nat. Neurosci. *2*, 1003–1009.

Kay, L.M., and Stopfer, M. (2006). Information processing in the olfactory systems of insects and vertebrates. Semin. Cell Dev. Biol. *17*, 433–442.

Lagier, S., Carleton, A., and Lledo, P.M. (2004). Interplay between local GABAergic interneurons and relay neurons generates gamma oscillations in the rat olfactory bulb. J. Neurosci. *24*, 4382–4392.

Lei, H., Christensen, T.A., and Hildebrand, J.G. (2004). Spatial and temporal organization of ensemble representations for different odor classes in the moth antennal lobe. J. Neurosci. *24*, 11108–11119.

Lin, D.Y., Zhang, S.Z., Block, E., and Katz, L.C. (2005). Encoding social signals in the mouse main olfactory bulb. Nature *434*, 470–477.

Lin, D.Y., Shea, S.D., and Katz, L.C. (2006). Representation of natural stimuli in the rodent main olfactory bulb. Neuron *50*, 937–949.

Macrides, F., and Chorover, S.L. (1972). Olfactory bulb units: activity correlated with inhalation cycles and odor quality. Science *175*, 84–87.

Mair, R.G. (1982). Response properties of rat olfactory bulb neurones. J. Physiol. *326*, 341–359.

Margrie, T.W., and Schaefer, A.T. (2003). Theta oscillation coupled spike latencies yield computational vigour in a mammalian sensory system. J. Physiol. *546*, 363–374.

Mazor, O., and Laurent, G. (2005). Transient dynamics versus fixed points in odor representations by locust antennal lobe projection neurons. Neuron *48*, 661–673.

McBride, K., and Slotnick, B. (2006). Discrimination between the enantiomers of carvone and of terpinen-4-ol odorants in normal rats and those with lesions of the olfactory bulbs. J. Neurosci. *26*, 9892–9901.

Meredith, M. (1986). Patterned response to odor in mammalian olfactory bulb: the influence of intensity. J. Neurophysiol. *56*, 572–597.

Mombaerts, P. (2004). Genes and ligands for odorant, vomeronasal and taste receptors. Nat. Rev. Neurosci. *5*, 263–278.

Mori, K., and Shepherd, G.M. (1994). Emerging principles of molecular signal processing by mitral/tufted cells in the olfactory bulb. Semin. Cell Biol. *5*, 65–74.

O'Keefe, J., and Burgess, N. (2005). Dual phase and rate coding in hippocampal place cells: theoretical significance and relationship to entorhinal grid cells. Hippocampus *15*, 853–866.

Perez-Orive, J., Mazor, O., Turner, G.C., Cassenaer, S., Wilson, R.I., and Laurent, G. (2002). Oscillations and sparsening of odor representations in the mushroom body. Science *297*, 359–365.

Rennaker, R.L., Chen, C.F., Ruyle, A.M., Sloan, A.M., and Wilson, D.A. (2007). Spatial and temporal distribution of odorant-evoked activity in the piriform cortex. J. Neurosci. *27*, 1534–1542.

Rinberg, D., Koulakov, A., and Gelperin, A. (2006a). Sparse odor coding in awake behaving mice. J. Neurosci. *26*, 8857–8865.

Rinberg, D., Koulakov, A., and Gelperin, A. (2006b). Speed-accuracy tradeoff in olfaction. Neuron *51*, 351–358.

Rubin, B.D., and Katz, L.C. (1999). Optical imaging of odorant representations in the mammalian olfactory bulb. Neuron *23*, 499–511.

Schaefer, A.T., Angelo, K., Spors, H., and Margrie, T.W. (2006). Neuronal oscillations enhance stimulus discrimination by ensuring action potential precision. PLoS Biol. *4*, e163.

Scott, J.W. (2006). Sniffing and spatiotemporal coding in olfaction. Chem. Senses *31*, 119–130.

Shang, Y., Claridge-Chang, A., Sjulson, L., Pypaert, M., and Miesenbock, G. (2007). Excitatory local circuits and their implications for olfactory processing in the fly antennal lobe. Cell *128*, 601–612.

Spors, H., Wachowiak, M., Cohen, L.B., and Friedrich, R.W. (2006). Temporal dynamics and latency patterns of receptor neuron input to the olfactory bulb. J. Neurosci. *26*, 1247–1259.

Stopfer, M., and Laurent, G. (1999). Short-term memory in olfactory network dynamics. Nature *402*, 664–668.

Stopfer, M., Jayaraman, V., and Laurent, G. (2003). Intensity versus identity coding in an olfactory system. Neuron *39*, 991–1004.

Uchida, N., and Mainen, Z.F. (2003). Speed and accuracy of olfactory discrimination in the rat. Nat. Neurosci. *6*, 1224–1229.

Verhagen, J.V., Wesson, D.W., Netoff, T.I., White, J.A., and Wachowiak, M. (2007). Sniffing controls an adaptive filter of sensory input to the olfactory bulb. Nat. Neurosci. *10*, 631–639.

Wachowiak, M., and Cohen, L.B. (2001). Representation of odorants by receptor neuron input to the mouse olfactory bulb. Neuron *32*, 723–735.

Wang, J.W., Wong, A.M., Flores, J., Vosshall, L.B., and Axel, R. (2003). Two-photon calcium imaging reveals an odor-evoked map of activity in the fly brain. Cell *112*, 271–282.

Wehr, M., and Laurent, G. (1999). Relationship between afferent and central temporal patterns in the locust olfactory system. J. Neurosci. *19*, 381–390.

Wiener, M.C., and Richmond, B.J. (1999). Using response models to estimate channel capacity for neuronal classification of stationary visual stimuli using temporal coding. J. Neurophysiol. *82*, 2861–2875.

Wilson, R.I., and Laurent, G. (2005). Role of GABAergic inhibition in shaping odor-evoked spatiotemporal patterns in the Drosophila antennal lobe. J. Neurosci. *25*, 9069–9079.

Wilson, R.I., Turner, G.C., and Laurent, G. (2004). Transformation of olfactory representations in the Drosophila antennal lobe. Science *303*, 366–370.

Yokoi, M., Mori, K., and Nakanishi, S. (1995). Refinement of odor molecule tuning by dendrodendritic synaptic inhibition in the olfactory bulb. Proc. Natl. Acad. Sci. USA *92*, 3371–3375.

Zou, Z., and Buck, L.B. (2006). Combinatorial effects of odorant mixes in olfactory cortex. Science (New York, N. Y *311*, 1477–1481.